1. Final Report on DoE Grant Number DE–AI02–01ER41170 with the Naval Research Laboratory.
2. Project Title: Development and Testing of Advanced Accelerator Structures and Technologies at 11.424 GHz, Steven H. Gold, PI, steven.gold@nrl.navy.mil, 202-767-4004.
3. Date of Report: 13 October 2013, covering the period 15 July 2010 – 14 July 2013.
4. The areas of activity are grouped by Task. Task 1 involved a study of the key physics issues associated with the use of high gradient dielectric-loaded accelerating (DLA) structures in rf linear accelerators, and was carried out in collaboration with Argonne National Laboratory (ANL) and Euclid Techlabs LLC; Task 2 involved a study of high-gain active microwave pulse compressors, and was carried out in collaboration with Omega-P, Inc. and the Institute of Applied Physics of the Russian Academy of Sciences. The experiments were carried out in the X-band Magnicon Laboratory at the Naval Research Laboratory (NRL). The studies under Task 1 were focused on multipactor and breakdown in externally driven DLA structures at the 200-ns timescale. Suppression of multipactor and breakdown are essential to the practical application of dielectric structures in rf linear accelerators. During the first year of this program, we carried out a study of a doubly tapered clamped quartz traveling-wave (TW) structure that operated at up to 15 MV/m without breakdown by eliminating dielectric joints, thus avoiding the joint breakdown that had characterized many earlier experiments. However, strong multipactor loading was observed in the structure. In the second year, we carried out a successful test of a TW DLA structure with a sputtered copper exterior coating that eliminated the need for a clamped metal enclosure to form the outer metallic boundary, thus simplifying the fabrication of the structure. In the second year, we also carried out the first test of a dielectric-loaded standing-wave (SW) accelerating structure. Multipactor loading limited the achievable accelerating gradient in the structure to 9 MV/m, but the SW structure proved to be a useful configuration for studying multipactor physics. To continue this study, a new standing-wave structure is in preparation that will permit direct measurements of the energy stored in the structure for new studies of multipactor physics. Finally, in the third year of the program, we focused on the suppression of multipactor loading using an applied axial magnetic field, as proposed by Chang *et al.* [C. Chang *et al., J. Appl. Phys.* **110**, 063304 (2011).]. Chang used an analytic model and PIC simulations to show that an axial magnetic field can reduce the period of the secondary electron trajectories on the dielectric surface, and thus spoil the multipactor resonance condition. The optimum effect occurs when the ratio of the gyrofrequency to the rf frequency is in the range of ~ 0.7 to 1. For an X-band structure, this is equivalent to a solenoidal field of 2.8–4 kG. This approach to multipactor suppression is attractive because it maintains the advantages of a DLA structure and is independent of other accelerator parameters.

An experimental test of multipactor suppression with an axial magnetic field was carried out at NRL on a TW DLA structure prepared by ANL and Euclid Techlabs. The structure consisted of an externally metalized alumina tube ($\varepsilon_r = 9.7$) enclosed in a copper housing to provide a vacuum seal and connected to input and output rf couplers. Fig. 1 (left) shows the geometry of the structure, which used tapered dielectric transitions at either end to match the impedance between the couplers and the accelerating section. The central beam channel was 8.53 mm in diameter. The structure operated in the traveling-wave TM_{01} mode, which has only three components: longitudinal electric field (E_z), radial electric field (E_r), and azimuthal magnetic field (H_ϕ). Fig. 1 (left) also shows the normalized amplitude of E_r and E_z along the structure, as well as a profile of the external magnetic field B_z produced by the solenoidal magnet. The accelerating gradient for this structure was 12.5 MV/m at 10 MW input power.

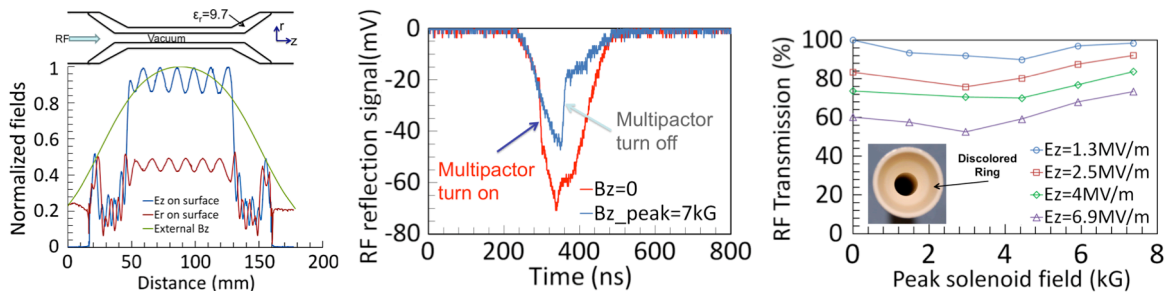

Fig. 1. (left) Sketch of the geometry of the alumina structure used in the experiment, along with the corresponding normalized rf electric fields and solenoidal magnetic field; (center) Comparison of the reflected rf signals at E_z=4 MV/m for B_z=0 kG and B_z=7 kG fields at center of the structure; (right) Measured rf transmission percent as a function of solenoidal field for different values of E_z. Inset shows discoloration on the disassembled input end of the structure, indicating that intense multipactor loading occurred in the tapered region of the dielectric tube.

The onset of multipactor has been shown to cause a decrease in the rf transmission through a structure, and is accompanied by the emission of light from the dielectric surface. In addition, the reflection coefficient of the structure may change. Fig. 1 (center) shows typical rf reflection signals measured by a diode detector in cases with and without an external magnetic field. The input rf pulse was approximately Gaussian in shape with a peak gradient of 4 MV/m. With B_z=0, the reflected signal increases sharply as the field rises above ~1 MV/m, indicating the onset of multipactor, while for B_z=7 kG, the abrupt rise in the reflected signal does not occur, and instead there is a sharp falloff in the reflected rf signal at a higher level of rf field. In addition, for B_z=7 kG, the multipactor light emission from the center of the structure, as observed by a video camera, was found to disappear and the rf transmission was improved. More generally, when a solenoidal magnetic field was applied, the effect was to either enhance or suppress the multipactor, depending on its field strength. Fig. 1 (right) plots the rf transmission of the DLA structure as a function of B_z for several different accelerating gradients. As predicted by theory, a weak solenoidal magnetic field enhanced the multipactor-induced rf loss, while a stronger field suppressed the multipactor for B_z in the optimal range. The data also showed that a higher accelerating gradient is favorable for multipactor suppression, which indicates the advantage of this approach for practical accelerator applications.

However, the data also showed that the rf transmission was not restored to the level that was measured before the onset of multipactor. Fig. 1 shows that for B_z=0, 40% of the rf power was absorbed when the accelerating gradient was increased from ~1 MV/m to ~7 MV/m, but that the transmission was only improved by ~15% at B_z=7 kG. The limited improvement that was observed is believed to be due to the variation of the axial magnetic field along the length of the structure, which resulted in an axially non-uniform effect on the multipactor suppression. This variation was caused by the large bore to length ratio of the available solenoid. Specifically, we observed apparent suppression of the multipactor discharge in the center section of the DLA structure (the multipactor light emission from that region vanished) when the peak value of solenoidal magnetic field was in the favorable range. However, multipactor was apparently greatly enhanced in the tapered regions of the dielectric structure, where B_z falls to half of its value in the center of the structure. This latter conclusion is supported by two additional observations. First, Fig. 1 (right inset) shows the presence of a discolored ring at the input end of the dielectric taper, indicating that intensified electron bombardment occurred in this region. Second, higher gas pressures were observed in the ion pumps located near both ends of the structure when higher values of B_z were applied. The enhanced level of multipactor in the two tapered transition regions would be expected to produce additional rf absorption, as was observed in the experiment.

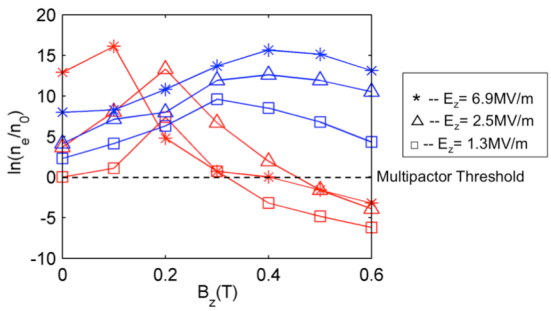

Fig. 2. Simulation of change in electron density (n_e/n_0) after 20 rf periods as a function of magnetic field (B_z) and rf field (E_z): Red curves--center of DLA structure; Blue curves--at taper. Note that all electric and magnetic field values correspond to the center of the structure.

The effect of an external magnetic field on multipactor in this structure was studied using the PIC code UNPIC (see Fig. 2). In the simulation model, a DC bias voltage was applied to provide a restoring field, equivalent to the space charge field of the secondary electron cloud, that satisfied the resonant condition $E_r/E_{dc}=\pi$. The parameters used in the simulation were f=11.42 GHz, initial rf phase φ=0, peak secondary electron yield (SEY) for normal incidence δ_{m0}=2.5, and electron energy at the peak ε_m=450 eV. The simulation followed the multipactor growth for 20 rf periods, beginning with an assumed initial electron density (n_0) that was chosen so that saturation would not occur during the simulation. The number of multipactor electrons was assumed to increase or decrease exponentially according to $n_e=n_0 \exp(t/\tau_b)$, where τ_b reflects the growth rate. Thus, the change in $\ln(n_e/n_0)$ shown in Fig. 2 can be used to characterize the rate of multipactor growth or suppression. As B_z was increased from 0 to 0.6 T, the red curves show that the multipactor growth in the center of the structure first increased, and then decreased at all values of E_z. It finally turning negative at the higher values of B_z, indicating multipactor suppression. However, because of the lower magnetic field in the tapered region of the structure, the multipactor growth in this region persisted at all values of the axial magnetic field, and was actually enhanced at the higher values. This is consistent with the experimental observations. A new TW DLA experiment is in preparation that will employ a longer solenoidal magnet to produce a uniform magnetic field throughout the test structure.

The experiments to date have characterized the properties of DLA structures at high levels of rf drive in order to study multipactor and breakdown phenomena. However, an additional goal of the program is to study actual acceleration in DLA structures. In order to prepare for these tests, ANL had previously arranged to have a 5-MeV X-band electron injector developed in China and delivered to NRL, where it was installed in a bunker in the Magnicon Laboratory (see Fig. 3 (left)). The injector is a 23½-cell disk and washer structure with a LaB_6 cathode that is designed to produce a ~5 MeV, 10 mA beam using ~5 MW of RF drive. Following the initial operation of the injector several years ago, there were difficulties with cath-

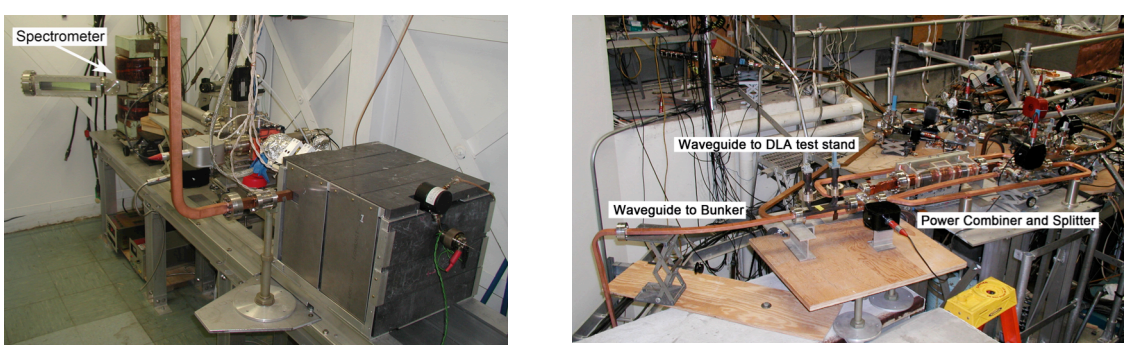

Fig. 3. (left) Beamline of X-band test accelerator, with magnetic spectrometer at far end; (right) Magnicon output waveguide switchyard, including power combiner and splitter assembly.

ode arcing that required the cathode to be replaced. A new cathode was installed and accelerator operation resumed in 2012. In addition, an electron spectrometer was installed at the end of the beam line to enable measurements of the electron energy, and was calibrated and tested. The magnicon output (see Fig. 3 (right)) includes an electrically controlled power splitter that can drive two separate waveguides with an adjustable power split ratio. Typically, all of the rf power is directed to a single waveguide, with one output normally used to power the 5 MeV accelerator and the second used to carry out rf tests of DLA structures. For the acceleration experiments, a new waveguide line was built to connect the second output into the bunker, so that the magnicon will be able to simultaneously power both the accelerator and a test structure that will be mounted between a pair of bellows at the end of the injector.

The planned tests will be the first studies of acceleration in an externally driven DLA structure, and will also help to diagnose the effect of multipactor, since the effective accelerating gradient measured by the electron energy gain can be compared to the predicted acceleration as a function of rf drive power. In order to produce time-resolved and quantitative data, a quartz window was put at the end of the output arm of the spectrometer, and a photomultiplier tube and scintillator were used to measure electrons deflected into the output arm as a function of magnetic field. Thus, all of the essential elements should now be ready to permit acceleration studies to be performed. The next step will be to insert a test structure into the beam line. A 20-cm structure at 10 MV/m should produce 2 MeV of acceleration, which can be readily measured. We plan to carry out acceleration tests using ANL/Euclid structures in the next year.

Task 2 of this grant covered the study of high power active microwave pulse compressors in collaboration with Omega-P, Inc. and the Institute of Applied Physics in Nizhny Novgorod, Russia. The study involved two-channel dual mode pulse compressors using electron-beam switching, and included two-month experimental runs in both 2012 and 2013. Fig. 4 shows a diagram of the experimental configuration used for the first run, as well as the operating mode in the switch cavities. The compressor consisted of two identical compressor channels that were fed through a 3-dB hybrid coupler that served to isolate the magnicon rf source from power reflected back from the compressor. Arm I of the hybrid connected to the magnicon, arms III and IV fed the compressor channels, and arm II was connected to the output load, with all the arms monitored by directional couplers. The compressor channels each consisted of a TE_{01} input and output section and a TE_{02} energy storage cavity, followed by a switch assembly that controlled the coupling between the TE_{01} and TE_{02} modes. The switch assembly included a conical taper that coupled the modes together, a TE_{01}-mode waveguide section, and an overcoupled TE_{012} switch cavity (see Fig. 4 (right)) connected to the waveguide through a diaphragm. The downstream wall of the switch cavity contained an annular slit to permit the entry of an electron beam that was produced from a knife-edged Mo cathode coated with a CVD diamond film that was driven by a –100 kV, 100 ns voltage pulse. In the initial state, the

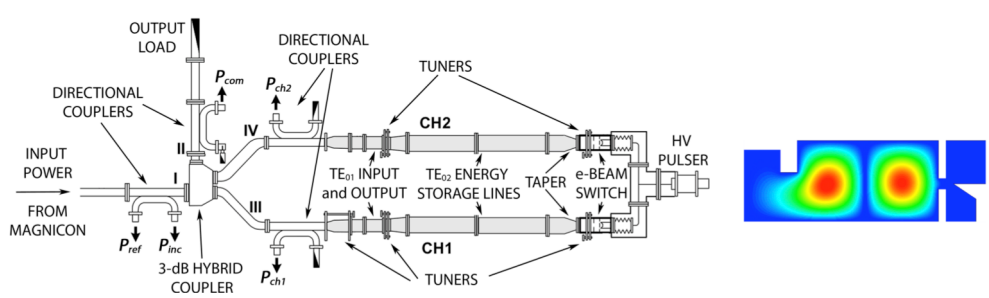

Fig. 4. (left) Diagram of high-power two-channel dual-mode active pulse compressor using electron-beam switching. (right) Cross-section of the switch cavity, showing coupling diaphragm, TE_{012} operating mode, and slit for injection of annular electron beam from knife-edge cathode at right.

switch cavity was in resonance, the reflection was out of phase, and the mode conversion was only ~2–3%, allowing the energy storage cavity to fill. When the electron beam was discharged into the switch cavity, the cavity was shifted out of resonance, causing the phase of the reflection to change by ~π. As a result, the mode coupling in the conical taper was greatly increased, and could approach ~100%. The increased coupling resulted in the discharge of the stored rf energy in one round trip of the TE_{02} mode in the energy storage cavity to produce a compressed rf output pulse. Effective switching requires that $n_e/n_c \sim 2/Q_S$, where n_e is the mean electron density in the cavity, $n_c \sim 1.6\times10^{12}$ cm^{-3} is the critical density at f=11.43 GHz, and $Q_S \sim$ 200–400 is the loaded quality factor of the switch cavity. This required a beam current in the range of 200 A – 400 A. The transition time of the switch cavity is $\tau_p \sim Q_S/2\pi f \sim$ 3–5 ns for $Q_S \sim$ 200.

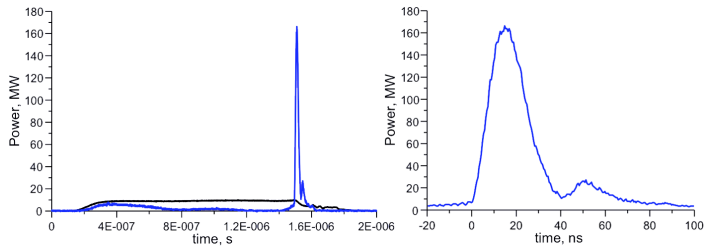

Fig. 5. (left) Oscilloscope traces of incident (black) and compressed (blue) output waveforms from the 2012 experimental run: P_{inc}=9.2 MW, P_{com}=165 MW, Gain=18.3; (right) Expanded view of output pulse.

Fig. 5 shows a set of oscilloscope traces from the 2012 experimental run. The left set of traces shows an incident 9.2 MW, ~1 μs drive pulse and the 165 MW, 19.8 ns FWHM output pulse. The pulse compression gain factor is 18.3. The right trace is an expanded view of the output pulse, showing that the energy storage cavity was almost completely discharged in a single cavity round trip time.

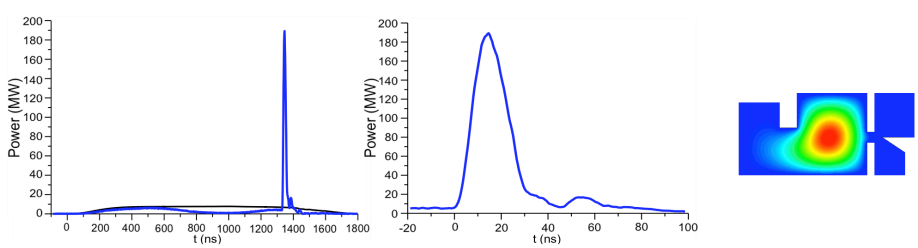

Fig. 6. (left) Oscilloscope traces of incident (black) and compressed (blue) waveforms from the 2013 experimental run: P_{inc}=7.4 MW, P_{com}=190 MW, gain=25.7; (center) Expanded view of output pulse; (right) Cross-section view of redesigned switch cavity, showing TE_{011} operating mode.

The purpose of the 2013 experiments was to test improved versions of the output switch that would enable higher gain operation, as well as to investigate several different versions of the cold Mo cathode, including uncoated versions and versions with different types of CVD-based diamond/graphite coatings. During these tests, still higher values of the gain were achieved. Fig. 6 (left) shows a 190 MW compressed pulse at 25.7 gain, using a 7.4 MW drive pulse from the magnicon, and Fig. 6 (right) shows the geometry and TE_{011} operating mode of the redesigned switch cavities. The compression efficiency in this case was ~50%. However, the switching gain began to decrease as the magnicon power was further increased, apparently because the ponderomotive force of the rf mode in the cavity interfered with the propagation of the electron beam that was used to shift the cavity resonant frequency. This suggested that a future experiment might require operation at higher cathode potential to reach higher peak

output powers. The success of these experiments shows a path to future high gain active versions of the SLED 2 pulse compressor at SLAC.

5. The following papers and presentations acknowledged the support of DoE:

   Journal articles:

   a. "Progress Toward Externally Powered X-Band Dielectric-Loaded Accelerating Structures," by C. Jing, W. Gai, J.G. Power, R. Konecny, W. Liu, S.H. Gold, A.K. Kinkead, S.G. Tantawi, V. Dolgashev, and A. Kanareykin, *IEEE Trans. Plasma Sci.*, vol. 38, no. 6, pp. 1354–1360, June, 2010.
   b. "Active Microwave Pulse Compressor Using an Electron-Beam Triggered Switch," by O.A. Ivanov, M.A. Lobaev, A.L. Vikharev, A.M. Gorbachev, V.A. Isaev, J.L. Hirshfield, S.H. Gold, and A.K. Kinkead, *Phys. Rev. Lett.*, vol. 110, 115002 (2013).

   Proceedings papers:

   a. "Development of X-Band Dielectric-Loaded Accelerating Structures," by S.H. Gold, C. Jing, A. Kanareykin, W. Gai, R. Konecny, J.G. Power, and A.K. Kinkead, in *Advanced Accelerator Concepts*: Proceedings of the Fourteenth Advanced Accelerator Concepts Workshop, 13–19 June 2010, Annapolis, MD, AIP Conference Proceedings 1299, edited by S.H. Gold and G.S. Nusinovich (American Institute of Physics Press, Melville, NY, 2010), pp. 292–296.
   b. "New Studies of X-Band Dielectric-Loaded Accelerating Structures," by S.H. Gold, C. Jing, S. Antipov, A. Kanareykin, W. Gai, R. Konecny, J.G. Power, and A.K. Kinkead, in Proceedings of the 2011 Particle Accelerator Conference, 28 March – 1 April 2011, New York, NY, pp. 337–339.
   c. "An X-band Standing Wave Dielectric Loaded Accelerating Structure," by C. Jing, S. Antipov, P. Schoessow, A. Kanareykin, R. Konecny, S. Kazakov, and S. Gold, in the Proceedings of the 2012 International Particle Accelerator Conference, 20–25 May 2012, New Orleans, LA, pp. 1927–1929.
   d. "Experiment on Multipactor Suppression in Dielectric-Loaded Accelerating Structures with a Solenoid Field," by C. Jing, R. Konecny, A. Kanareykin, S. Antipov, P. Schoessow, C. Chang, L. Xiao, L. Ge, M. Conde, J.G. Power, W. Gai, and S. Gold, in the Proceedings of IPAC 2013, The 4th International Particle Accelerator Conference, 12–17 May 2013, Shanghai, China, paper TUPEA087.

   Additional presentations:

   a. "Experimental Studies of Active RF Pulse Compression," by O.A. Ivanov, A.A. Vikharev, A.M. Gorbachev, V.A. Isaev, M.A. Lobaev, A.L. Vikharev, S.V. Kuzikov, M.A. Lapointe, S.V. Shchelkunov, S.H. Gold, A.K. Kinkead, S.G. Tantawi, V.A. Dolgashev, and J.L. Hirshfield, presented at the X-Band RF Structures, Beam Dynamics, and Sources Workshop, 20 November – 3 December 2010, Cockcroft Institute.
   b. "High power test of active microwave pulse compressor with switch employing electron beam triggering," by O.A. Ivanov, A.L. Vikharev, M.A. Lobaev, A.M. Gorbachev, V.A. Isaev, J.L. Hirshfield, S.H. Gold, and A.K. Kinkead, presented at Strong Microwaves and Terahertz Waves: Sources and Applications, 9–16 July 2011, Nizhny Novgorod, Russia.
   c. "High Power X-band Pulse Compressor Using Electron Beam Switching," by Anatoly L. Vikharev, Aleksey M. Gorbachev, Oleg A. Ivanov, Mikhail Lobaev, Steven H.

Gold, Jay L. Hirshfield, and Allen K. Kinkead, presented at the Fifteenth Advanced Accelerator Concepts Workshop—AAC 2012, 10–15 June 2012, Austin, TX.

d. "Test of an X-band Standing Wave Dielectric Accelerating Structure," by C. Jing, S. Antipov, P. Schoessow, A. Kanareykin, J. Power, M. Conde, W. Liu, R. Konecny, W. Gai, S.H. Gold, C. Chang, V. Dolgashev, and S. Tantawi, presented at the Fifteenth Advanced Accelerator Concepts Workshop—AAC 2012, 10–15 June 2012, Austin, TX.

e. "Active X-Band Pulse Compressor Using Electron-Beam Switching," by S.H. Gold, A.L. Vikharev, A.M. Gorbachev, O.A. Ivanov, M. Lobaev, and A.K. Kinkead, presented at the Thirty-Ninth IEEE International Conference on Plasma Science, 8–12 July 2012, Edinburgh, UK.

f. "Active Pulse Compression Results," by A.L. Vikharev, O.A. Ivanov, M.A. Lobaev, A.M. Gorbachev, V.A. Isaev, J.L. Hirshfield, S.H. Gold, and A.K. Kinkead, presented at HG2013: International Workshop on Breakdown Science and High Gradient Technology, 3–6 June 2013, Trieste, Italy.

h. "Effect of an Axial Magnetic Field on Multipactor in a Dielectric-Loaded Accelerating Structure," by S.H. Gold, C. Jing, W. Gai, A. Kanareykin, and A. Kinkead, presented at the IEEE Pulsed Power & Plasma Science Conference — PPPS 2013, 16–21 June 2013, San Francisco, CA.

i. "Test of a Standing Wave Dielectric Loaded Accelerating Structure," by C. Jing, S.P. Antipov, A. Kanareykin, P. Schoessow, W. Gai, and S.H. Gold, presented at the 2013 North American Particle Accelerator Conference, NA-PAC 2013, 29 September – 4 October 2013, Pasadena, CA.

j. "High Gradient Research at the Naval Research Laboratory," by Steven H. Gold, seminar presented at Purdue University, West Lafayette, IN, 21 September 2011.

6. The following individuals received support from this project:
   Steven H. Gold, PI—50% support.
   Allen K. Kinkead, research engineer—25% support.
   No personnel transitions occurred.